FIIGHT PATH FOLLOWING GUIDANCE FOR UNMANNED AIR VEHICLES WITH PAN-TILT CAMERA FOR TARGET OBSERVATION

Sebastian Stolle, Rolf Rysdyk, University of Washington, Seattle, WA

Abstract

An Unmanned Autonomous Vehicle (UAV) is equipped with a nose-mounted camera capable of pan and tilt rotation for the observation of ground targets. The two camera angles are adjusted automatically in order to keep the target in the camera's field of view. While the camera actuators are fast enough to keep up with vehicle motion, the limited range of the camera angles leads to the target getting out of sight. Therefore, target exposure is affected by wind. Furthermore, the relative position of the sun can lead to glare and image overexposure. While the effect of wind can be improved by commanding a sideslip angle, image overexposure is avoided by keeping the vehicle between sun and target. Thus, it is desirable to define maneuvers that result in maximum target exposure, and provide guidance laws to allow path following for these maneuvers. This paper presents initial results, obtained based on circular and elliptical maneuvers. The results were generated using an accurate non-linear Aerosonde UAV representation and environmental dynamic models. Simulated GPS data was used for the path following guidance. The complete path about the target at constant altitude and airspeed is specified simply by the desired orbital segment and course reversals at the segment boundaries. With camera pan limited to the forward 180^o, this can achieve long term observation. A camera with minor 'look-back' range can provide continuous observation in a maneuver that employs both circular and elliptical segments.

Introduction

Unmanned Autonomous Vehicles (UAVs) are suitable for tasks that do not require or allow the presence of a human operator on the vehicle. An advantage of UAVs is that they can cope with a wider range of motion frequencies, damping ratios, and accelerations than a human, especially when the payload is small. One of the useful applications is remote observation, for which the payload consists of a camera mounted to the vehicle.

The purpose of this work is to develop flight path guidance for a UAV equipped with a nose-mounted camera that has two degrees of freedom, pan and tilt rotation. Inner control loops providing basic autopilot functions such as airspeed hold, altitude hold, and turn coordination, are assumed.

Different orbits about the target are explained and investigated. Problems regarding the camera field of view and possible solutions are discussed. An important objective is to minimize heuristics so that solutions rely on few parameters, e.g. vehicle and target position. The results take realistic weather situations into account, e.g. gusty winds. The flight path guidance law is tested with an accurate nonlinear dynamic model [2] of the Aerosonde [3], [4]. In the assessment of this work both vehicle guidance and camera pointing algorithms are based on GPS data, the camera pointing algorithm relies on aircraft attitude information. Nomenclature is provided at the end of this paper.

Assumptions, Definitions, Geometry, and Kinematics

The vehicle is provided with basic autopilot functions, it maintains altitude by means of an auto-throttle, and airspeed is maintained by means of a pitch autopilot. Prevalent wind information is available. Therefore, the analytical assumptions are:

1 The vehicle maintains altitude.
2 The airspeed is constant.
3 Average wind speed and direction are known.

Demanded Course

When flying on a circular path, the demanded course (flight path direction) is related to the

clock-angle (relative bearing from the target) as

$$\chi_{dem,cw} = \Psi_P + \frac{\pi}{2} \quad (1)$$

$$\chi_{dem,cc} = \Psi_P - \frac{\pi}{2} \quad (2)$$

where index 'cw' is a clockwise circle, and 'cc' a counter clockwise circle.

Demanded Camera Angles

In order to describe the movement of the 2-degree-of-freedom camera, a reference frame (index 'cam') is assigned to the camera itself. The x_{cam}-axis always points along the line of sight, whereas the y_{cam}- and z_{cam}-axis define the image that is taken by the camera. The transformation from the body to the camera reference frame is defined as a series of two rotations involving a pan angle λ and a tilt angle κ. In the case of the line of sight being parallel to the body-x-axis, $\lambda = \kappa = 0$. This is illustrated in figure 1, which shows the reference frame involving the camera angles κ (tilt) and λ (pan). The sequence of rotations is defined as

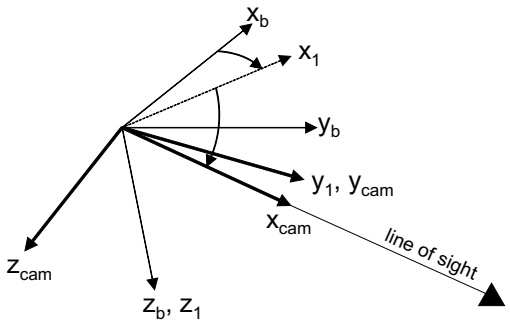

Figure 1 Transformation Body to Camera.

pan followed by tilt, leading to the following matrix for the transformation from body to camera reference frame:

$$T_{camb} = \begin{bmatrix} \cos\kappa\cos\lambda & \cos\kappa\sin\lambda & \sin\kappa \\ -\sin\lambda & \cos\lambda & 0 \\ -\sin\kappa\cos\lambda & -\sin\kappa\sin\lambda & \cos\kappa \end{bmatrix} \quad (3)$$

The equations describing the two camera angles are found by expressing the line of sight vector $\vec{los}$ in both camera and earth reference frame and transforming the expressions to the body reference frame. In the camera reference frame, $\vec{los}$ is

$$\vec{los}|_{cam} = r \cdot \begin{bmatrix} 1 \\ 0 \\ 0 \end{bmatrix}_{cam} \quad (4)$$

where r is a factor that defines the length of the line of sight. This vector is transformed to the body reference frame by the transpose of T_{camb}. The

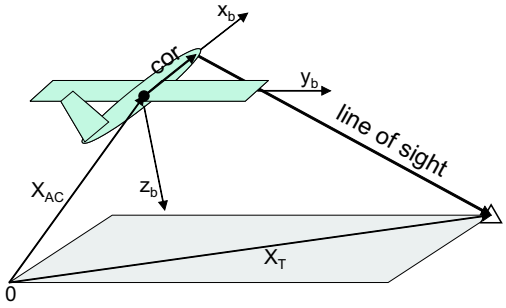

Figure 2 The Line of Sight Vector

expression for $\vec{los}|_g$ is obtained from figure 2, which shows that the line of sight depends on the target and vehicle positions, $\vec{X}_T$ and $\vec{X}_{AC}$, as well as the camera's center of rotation, $\vec{cor}$. This vector is expressed in body coordinates and, therefore, has to be transformed to the earth reference frame. The equation obtained from the figure is:

$$\vec{los}|_g = \vec{X}_T - \vec{X}_{AC} - T_{gb} \cdot \vec{cor} \quad (5)$$

This expression is transformed to the body reference frame by the transformation matrix $T_{bg} = T_{bg}(\Phi, \Theta, \Psi)$. The factor r in equation 4 represents the length of the line of sight and is replaced by the absolute value of the right hand side of equation 5. Equations 4 and 5 lead to the following vector equation:

$$\begin{bmatrix} \cos\kappa\cos\lambda \\ \cos\kappa\sin\lambda \\ \sin\kappa \end{bmatrix}_b = T_{bg} \cdot \frac{\vec{X}_T - \vec{X}_{AC} - T_{gb} \cdot \vec{cor}}{|\vec{X}_T - \vec{X}_{AC} - T_{gb} \cdot \vec{cor}|} \quad (6)$$

From these expressions the unknown values κ and λ are determined. Let $[a, b, c]^T$ represent the normalized vector $\vec{X}_T - \vec{X}_{AC} - \vec{cor}$ when expressed in the body reference frame, the demanded camera angles are then:

$$\kappa_{dem} = \arcsin(c) \quad (7)$$

$$\lambda_{dem} = \arctan(b/a) \quad (8)$$

These expressions do not take camera dynamics into consideration. However, due to their high bandwidth, the camera actuators are easily capable of keeping up with the motion of the vehicle.

Minimum Radius

The minimum radius of the circle about the target that can be achieved depends on: the inertial velocity V_c; the bank angle Φ, and the sideslip angle β. For calculating the minimum possible radius of the circle, the side-slip is assumed to be suppressed, i.e. the aircraft is assumed to be in a coordinated turn, which implies that the radius R is then:

$$R = \left| \frac{V_c^2}{g \cdot \tan \Phi} \right| \tag{9}$$

A higher inertial velocity increases the radius whereas a larger bank angle decreases it. Since the inertial velocity is the sum of airspeed and wind speed, there will always be a maximum $V_{c,max} = |V_a| + |V_w|$ at one point of the circle. In order to ensure that the vehicle can stay on the circular path, this maximum inertial velocity has to be used for calculating the demanded radius. There are also limits to the possible bank angle. Therefore, Φ_{max} will be used for the minimum radius.

$$R_{min} = \left| \frac{(|V_a| + |V_w|)^2}{g \cdot \tan \Phi_{max}} \right| \tag{10}$$

This value can be calculated before entering the circular path, but should be updated when airspeed or wind speed change significantly.

Approaching the Target

The target object can be approached from an a-priori specified course. GPS data is used to determine the flight path, the horizontal distance from the target, and the relative bearing. Flight path values obtained from GPS data have the advantage of being independent of wind data. Directly approaching the target means that the vehicle has to fly on a straight line with a constant demanded course χ_{dem}. The target coordinates and the demanded approach course define the approach path, which is a line in the x_g-y_g-plane.

$$\begin{bmatrix} \sin \chi_{dem} \\ -\cos \chi_{dem} \end{bmatrix} \cdot \begin{bmatrix} x \\ y \end{bmatrix} = x_{g,T} \sin \chi_{dem} - y_{g,T} \cos \chi_{dem}$$

Inserting the GPS coordinates of the vehicle's position P_{AC} into the x and y values of this equation, provides the shortest distance Δy between the vehicle and the desired flight path. The expression for Δy is also multiplied by -1 so that values of Δy are negative when the vehicle is to the left of the desired flight path when viewed from above in the direction of flight:

$$\begin{aligned} \Delta y \;\; = \;\; & \sin \chi_{dem} \cdot (x_{g,T} - x_{g,AC}) + \\ & \cos \chi_{dem} \cdot (y_{g,AC} - y_{g,T}) \end{aligned}$$

Now the deviation from the desired flight path can be parameterized by the two values

- Δy: determines the distance from the desired path
- $\Delta \chi$: determines the course deviation

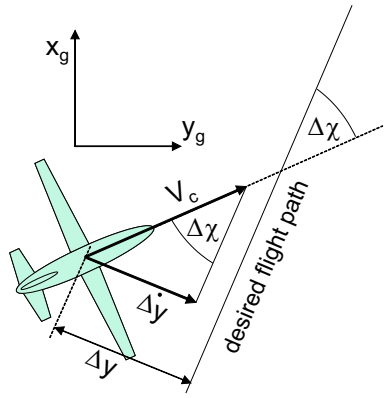

Figure 3 Deviation Geometry

According to figure 3, a change in Δy can be accomplished by a change in χ with the following approximation:

$$\Delta \dot{y} = V_c \cdot \Delta \chi \tag{11}$$

The normal procedure for changing the flight path direction is to bank the vehicle and suppress the resulting sideslip. The relation between the change in flight path and the bank angle is:

$$\dot{\chi} = \frac{g}{V_c} \cdot \tan \Phi \tag{12}$$

This means that deviations from the desired flight path are reduced by commanding a $\dot{\chi}$, which is based on Δy and implemented by means of a commanded bank angle. When used for feedback, though, the parameters $\Delta\chi$ and Δy can introduce problems which require special attention. Since the values of χ are bound to the interval $[0 \ldots 360^o]$, the calculation of $\Delta\chi$ depends on whether $|\chi - \chi_{dem}|$ is greater or smaller than 180^o. Thus, the two equations for $\Delta\chi$ are:

$$\Delta\chi = \chi - \chi_{dem} \quad \text{for} \quad |\chi - \chi_{dem}| \leq \pi \tag{13}$$

$$\Delta\chi = (2\pi - |\chi - \chi_{dem}|) \cdot sgn(\chi - \chi_{dem}) \quad \text{for} \quad |\chi - \chi_{dem}| > \pi \tag{14}$$

The vehicle is supposed to approach the desired flight path on a 45^o intercept course and smoothly bank to capture the desired path without overshoot and exceeding the maximum bank angle. This may be achieved by modelling of 'Helmsman Behavior' [6], [7], which is a form of output redefinition that couples a commanded course to cross-distance. Figure 4 illustrates this behavior. The commanded course deviation $\Delta\chi_{com}$ is a function of the distance Δy from the desired flight path, with saturation at $\Delta\chi_{com} = \pm 45^o$. The

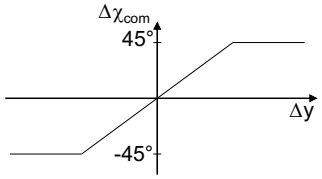

Figure 4 Model of Helmsman Behavior

function between the two saturation levels is:

$$\Delta\chi_{com} = \frac{k_y}{V_c}\Delta y \tag{15}$$

where k_y is a constant gain that determines how aggressively the vehicle reacts to a deviation Δy. For the given vehicle, the gain $k_y = \frac{45}{4} \cdot \frac{\pi}{180}$ has been found to produce a response that allows smooth convergence to $\Delta y = 0$ while meeting the mentioned requirements. The control loop architecture for capturing and holding a commanded flight path is shown in figure 5. With this architecture the demanded flight path can be captured from any given initial position and held

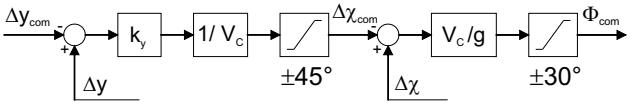

Figure 5 Guidance Loop Architecture

even with strong side wind. In addition to that, the vehicle can follow a commanded distance from the path Δy_{com}, which will prove useful when capturing the circular path around the target.

Circular Path about the Target

The path following guidance derived in the previous section is applicable on any smooth path including a circle about the target. The parameters for the circle are similar to that of the straight line path. The difference is, that χ_{dem} changes according to the position of the vehicle relative to the target, Ψ_P. The distance from the path, Δy, is substituted by a ΔR, which is:

$$\Delta R_{cw} = R_{dem} - R \tag{16}$$

$$\Delta R_{cc} = R - R_{dem} \tag{17}$$

The demanded path angle for the circular path was determined in equations 1 and 2. Figure 6 shows the corresponding block diagram. The guidance law

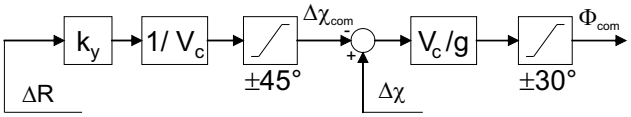

Figure 6 Architecture for Capturing and Holding a Circular Path

as presented allows for smooth path following for any sequence of path-segments [7]. However, for demonstration purposes, the transition between the straight and circular path segments can be automated by switching at a specified radius R_{switch}, which has to be greater than the demanded radius of the circle. If R_{switch} is too small, the vehicle will be likely to leave the circle when large disturbances occur. On the other hand, if R_{switch} is very large it will take more time until the vehicle converges with the desired circular path. A good compromise is $R_{switch} = 1.5 \cdot R_{dem}$. Figure 7

shows the ground track of a complete circular flight path including the approach. $V_a = 30m/s$, $V_w = 5m/s$, $\Psi_w = 90^o$, initial heading $\Psi(0) = 360^o$. Only target position and desired approach direction are used.

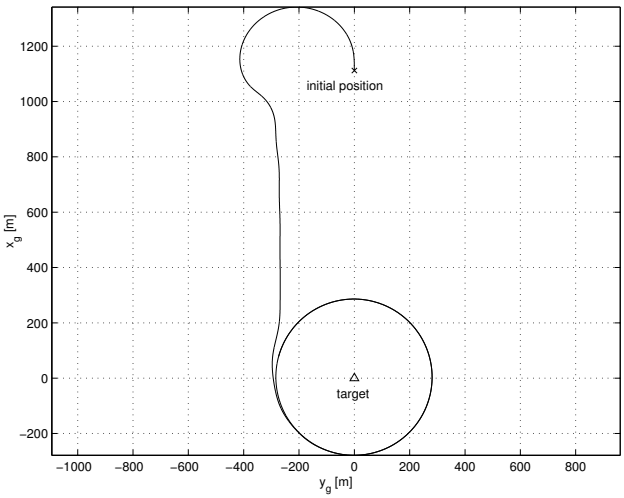

Figure 7 Simulated Ground Track of Circular Path about Target in Wind

Camera Field of View

Limited Camera Angles

Analytic expressions for the camera angles κ and λ have already been found in the geometry section (equations 7 and 8). With these expressions, the demanded camera angles can be calculated for any position and attitude of the vehicle. However, there are mechanical limits to these angles which can cause the camera image not to be focused on the target when flying in wind. With a nose-mounted camera setup, it is very likely that the camera can only point in a mainly forward direction, because the view in the backward direction is blocked by the vehicle itself. A very conservative specification of the mechanical limits to κ and λ is:

$$0 \leq \kappa \leq 90^o$$
$$-90^o \leq \lambda \leq 90^o$$

Figure 8 shows κ_{dem} (top) and λ_{dem} (bottom) on the circular path with $V_a = 30m/s$, $V_w = 5m/s$, $\Psi_w = 90^o$, including mechanical limits to the

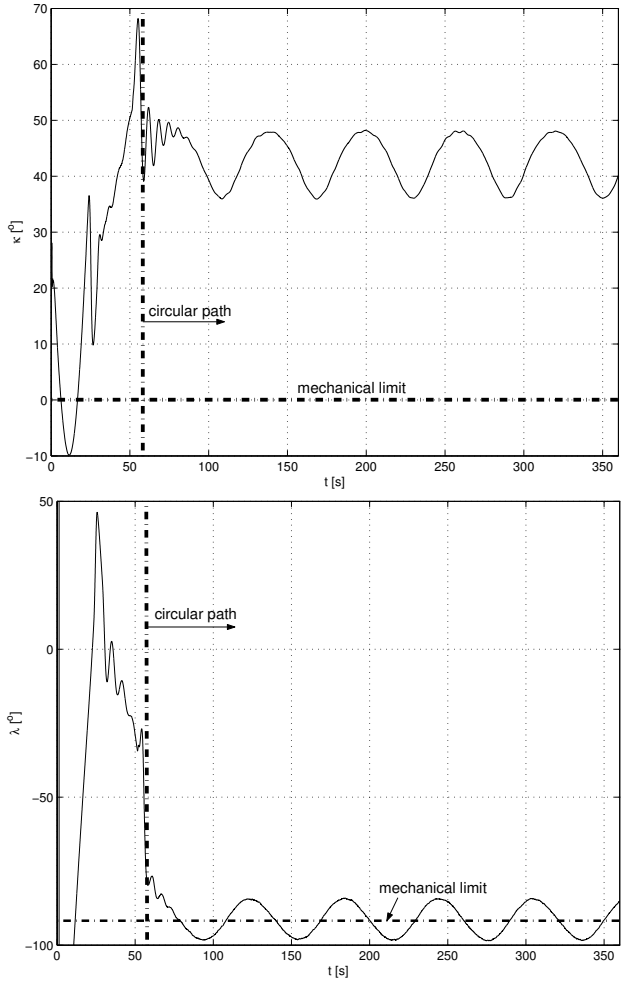

Figure 8 Time History of Demanded Camera Angles

camera angles. The tilt angle κ_{dem} stays within its limits on the circular path. The demanded pan angle λ_{dem}, on the other hand, periodically exceeds the mechanical limit. The result of this is illustrated in figure 9, which shows 9 snap shots of the camera field of view, taken at an interval of 5 seconds from an altitude of 500m above the target. The camera view is assumed to be cone-shaped with a zoom angle of 10^o. Three of these snap shots do not contain the target object. It is desirable, though, to have the target in sight during the entire maneuver.

A Solution

The problems with camera view are caused by heading adjustments when flying in wind. Changing

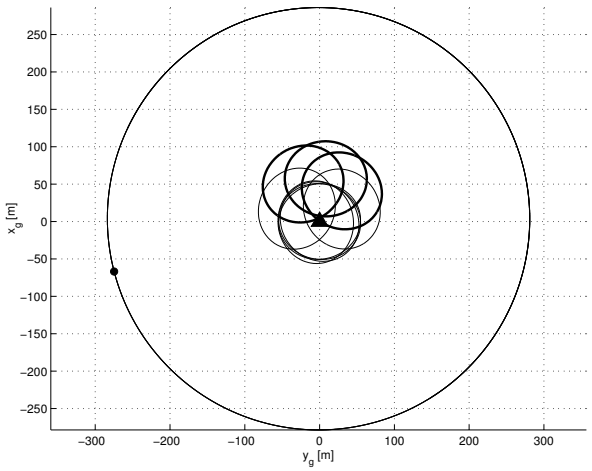

Figure 9 Ground Track and 9 Snapshots of Camera Field of View

the heading back to where it would be without wind can therefore bring the target back in sight. It is important, though, to change the orientation of the vehicle relative to the target without compromising flight path following. The use of a bank angle command to change heading and improve observation of the target is therefore not possible. A more suitable method to achieve a change in heading is commanding a sideslip angle. Figure 10 shows this effect of β on the camera view, with the target at the origin. The top traces show the target gets back in sight with $\beta = 4^o$; the bottom traces show a nearly centered view of the target with $\beta = 8^o$. However, sideslip will also increase drag and fuel consumption. A simulation with the Aerosonde model shows that fuel consumption when flying with a sideslip angle of 8^o is increased by about 15.7% compared to flying without sideslip. This poses a problem to long term observation because of the very limited amount of fuel that can be carried by UAV. To minimize the negative and maximize the positive effects of β, it makes sense to only use sideslip when it is needed and at the appropriate magnitude.

Quantitative Effect of Sideslip and Variable Sideslip Command

An analytic expressions that expresses β in terms of λ is not possible, since λ depends on bank

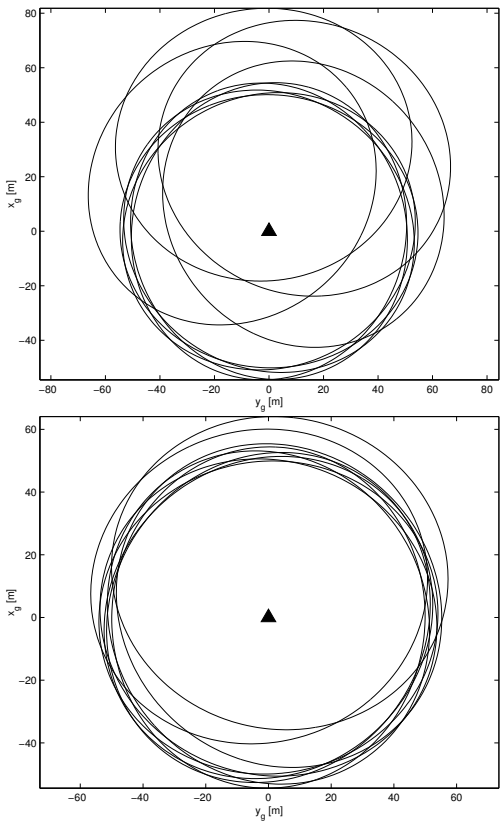

Figure 10 Effect of Sideslip on Camera Field of View

angle and the heading, which cannot be solved for analytically. Without an analytic expression, a variable sideslip command might be constructed from the difference between demanded and mechanically limited pan angle. This error can then be used for feedback to a commanded sideslip. However, simulation quickly showed that this feedback loop defeats its purpose; the relatively large inertia about the z_b-axis and low control authority prevents the vehicle from quickly responding to the sideslip commands. A small delay or overshoot results in a lightly damped fast oscillatory motion about the z_b-axis. On the circular path, the sideslip command changes frequently. The oscillatory behavior makes this a poor solution. Two other approaches are either to follow an a-priori calculated β_{com}, which can be implemented numerically, or to fly with no sideslip at all.

Circle-based Maneuvers

Advantage and Disadvantage of the Circular Path

The parameterization of the circular path discussed in the previous section is not very complex, which makes this maneuver a very robust one for the path following guidance developed above. It has been mentioned, though, that with very limited range of camera motion the camera may lose sight of the target when flying in the circle segment where Ψ_P is close to Ψ_w. The segment of the circle where $\Psi_P \in [\Psi_w - (\pi/4) \ldots \Psi_w + (\pi/4)]$ should therefore be avoided in this case. The wind direction poses less of a problem when the pan angle is allowed to be greater than 90^o.

In addition to wind, the position of the sun has to be taken into consideration, too. The circular path always contains a segment where the target is between the vehicle and the current position of the sun Ψ_S. In this segment, the quality of the camera images is drastically reduced due to overexposure. The segment of the circular path where $\Psi_P \in [\Psi_S + 3\pi/4 \ldots \Psi_S + 5\pi/4]$ should thus be avoided, independent of what the limits of camera motion are. Hence, depending on the camera limits, the usable segment of the circle about the target object has a minimum size of 90^o and a maximum size of 270^o. In the following, maneuvers for both cases of either very strict camera limits or wider range of camera motion will be discussed and compared.

Segmented Circular Orbit and Course Reversals

Case 1: $|\lambda| \leq 90^o$

In the case of the camera pan angle being limited to $|\lambda| \leq 90^o$, both the circular segment with image overexposure due to direct sunlight and the segment close to wind direction have to be avoided, if possible. These two undesirable segments can either form one large segment with at least half of the circle usable for maneuvers, or two separate segments, leaving two small usable segments. In the worst case, these two usable segments are equal

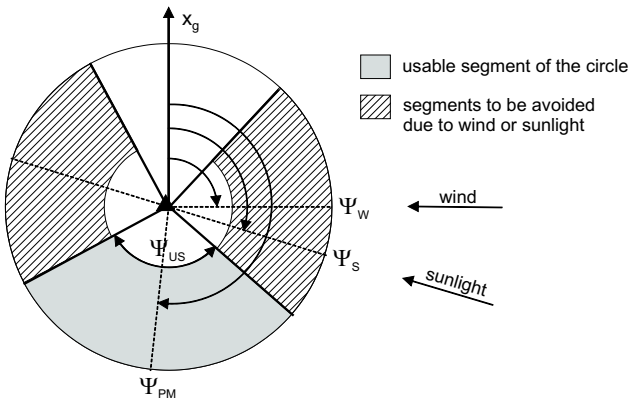

Figure 11 Segment Usable and To-Be-Avoided According to Wind Direction and Sun Position

in size, each containing a quarter of the circle. It is more likely, though, that one of the usable segments is greater than the other with a size ranging between 90^o and 180^o. Figure 11 illustrates this setting. The larger segment is, the more favorable it is for maneuvers, because sharp turns have to occur less often, thus avoiding steeply banked turns and potential problems for the camera field of view.

The usable segment of the circle about the target is defined by its middle position (relative bearing from the target) Ψ_{PM} and its size Ψ_{US}. The middle position Ψ_{PM} is determined with the mean value of the center of the segments to be avoided, Ψ_w and $\Psi_S + \pi$.

$$\begin{aligned} \Psi_{PM} &= \tfrac{\Psi_S + \pi + \Psi_w}{2} \quad \text{for} \quad \Psi_S \geq \Psi_w \\ \Psi_{PM} &= \tfrac{\Psi_S + \pi + \Psi_w}{2} - \pi \quad \text{for} \quad \Psi_S < \Psi_w \end{aligned}$$

The size of the usable segment is determined by:

$$\begin{aligned} \Psi_{US} &= \Psi_S - \Psi_w + \frac{\pi}{2} \quad \text{for} \quad \Psi_S \geq \Psi_w \\ \Psi_{US} &= \frac{3}{2}\pi - |\Psi_S + \pi - \Psi_w| \\ &\quad \text{for} \quad \Psi_S < \Psi_w \end{aligned}$$

Thus, the boundaries of the usable segment are $\Psi_{lim\pm} = \Psi_{PM} \pm \frac{1}{2}\Psi_{US}$.

Case 2: $|\lambda| \leq 110^o$

In the case of wider range of camera motion, the undesirable segment caused by wind influence

does not have to be considered in the parameterization of the usable segment. The middle position of the usable segment is then the same as the position of the sun.

$$\Psi_{PM} = \Psi_S \tag{18}$$

The size of the usable segment remains constant for all Ψ_S.

$$\Psi_{US} = \frac{3}{2}\pi \tag{19}$$

This size, though, does not have to be used completely as long as the chosen maneuver provides long term observation.

Maneuvers

Case 1: Circle Segment with One Radius (CS1R)

The first maneuver to be discussed consists of a circular path about the target with a course reversal at each boundary of the usable segment. The vehicle is supposed to turn towards the target to keep the camera field of view on the target as long as possible, and return to the same circle radius R_{dem}. The path following guidance law requires a parameterization of the desired path with the demanded flight path angle χ_{dem} and its rate and position information. For the proposed maneuvers these parameters have to be found.

Since wind direction, position of the sun, and relative bearing from the target are all given as angles between 0 and 2π, the notation $[\dots]_{2\pi}$ will be used for all angles bound to the interval between 0 and 2π.

For the CS1R maneuver, the demanded radius R_{dem} is a constant, similar to the full circle maneuver. However, this constant has to be large enough to provide that course reversals with a 30^o bank angle are possible. An expression for the demanded flight path angle on a (segment of a) circle has been found with equations 1 and 2. These equations can be generalized by the expression:

$$\chi_{dem} = \Psi_P + SGN \cdot \frac{\pi}{2} \tag{20}$$

where SGN is either -1 or 1, depending on the following conditions:

1) the direction, in which the vehicle is currently moving (cw or cc)
2) the difference between the current position of the vehicle and the boundary of the usable circle segment
3) the shortest way to the usable segment, if outside of the boundaries
4) the difference between the two boundary values
5) the difference between the middle position of the usable segment and its opposite position $[\Psi_{PM} + \pi]_{2\pi}$

This parameterization ensures that the vehicle finds the usable segment and changes its flight path direction by 180^o as soon as it crosses the boundary leaving the usable segment. The course reversal is supposed to be performed with a heading towards the target. This is done by applying a forced $\pm 30^o$ bank angle command whenever $|\Delta\chi| > 150^o$. The sign of the bank angle command has to be the opposite of the sign in equation 20.

$$\Phi_{com} = -SGN \cdot 30^o \quad \text{for} \quad |\Delta\chi| > 150^o \tag{21}$$

The resulting ground track is shown in figure 12,

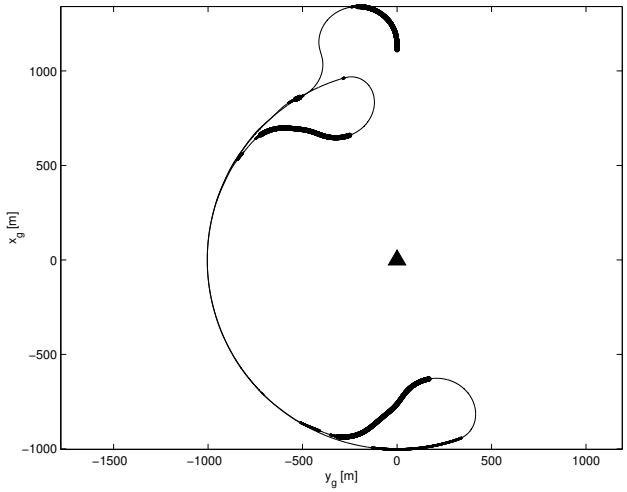

Figure 12 Simulated Ground Track of CS1R

with highlighting according to the quality of the camera images: centered view of the target (thin line), non-centered view of the target (medium line), target not in sight (thick line), $V_a = 30m/s$, $V_w = 5m/s$, $\Psi_S = 235^o$, $\Psi_w = 90^o$. When the vehicle returns to the demanded radius, the target is

out of sight for a certain time. This occurs at each course reversal due to returning to the same circle radius and limits the continuous exposure to the time that the vehicle takes from one course reversal to the next. One solution which extends the continuous exposure time would be to use two different radii when flying clockwise and counterclockwise.

Case 1: Circle Segment with Two Radii (CS2R)

This maneuver involves one demanded radius R_{cw} for clockwise flight about the target and a demanded radius $R_{cc} \neq R_{cw}$ for counterclockwise flight. Whether the clockwise radius is chosen to be the greater radius R_{out} depends mostly on the wind-sun-setting. Since one of the two course reversals will definitely cause a loss of sight of the target, this one can also be closer to the segment to be avoided due to wind in order to ensure that the other course reversal is not negatively affected by wind. In the example simulation, Ψ_w is set to 90^o (wind from East), and Ψ_S is set to 235^o (afternoon on the northern hemisphere). Thus, the outer radius is chosen to be the radius for clockwise flight ($R_{out} = R_{cw}$).

The parameterization of the flight path angle χ_{dem} is the same as for the CS1R maneuver, because the course reversals have to be performed at the exact same boundaries. The parameter for the radius has to be switched according to the sign SGN in equation 20. In this example:

$$R_{dem} = R_{out} \quad \text{for} \quad SGN = 1 \tag{22}$$

$$R_{dem} = R_{in} \quad \text{for} \quad SGN = -1 \tag{23}$$

Figure 13 shows the ground track of the CS2R maneuver, with highlighting according to the quality of the camera images: centered view of the target (thin line), non-centered view of the target (medium line), target not in sight (thick line), $V_a = 30m/s$, $V_w = 5m/s$, $\Psi_S = 235^o$, $\Psi_w = 90^o$. The time of continuous target observation is significantly increased compared to the CS1R maneuver. Another advantage of the CS2R maneuver is the increased amount of information contained in the images due to the reduced distance from the target when flying on the inner radius.

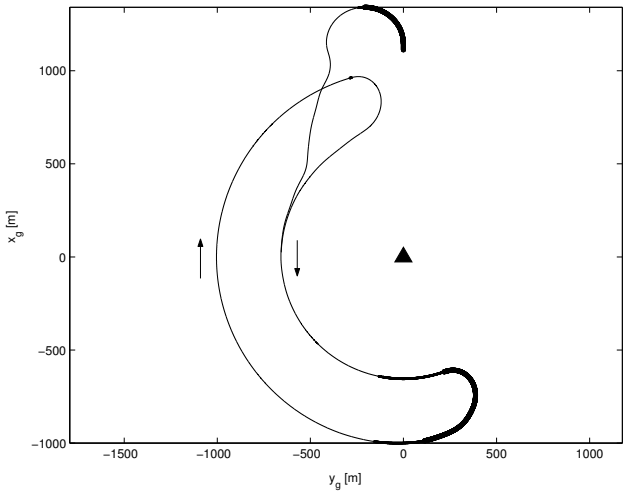

Figure 13 Simulated Ground Track of CS2R

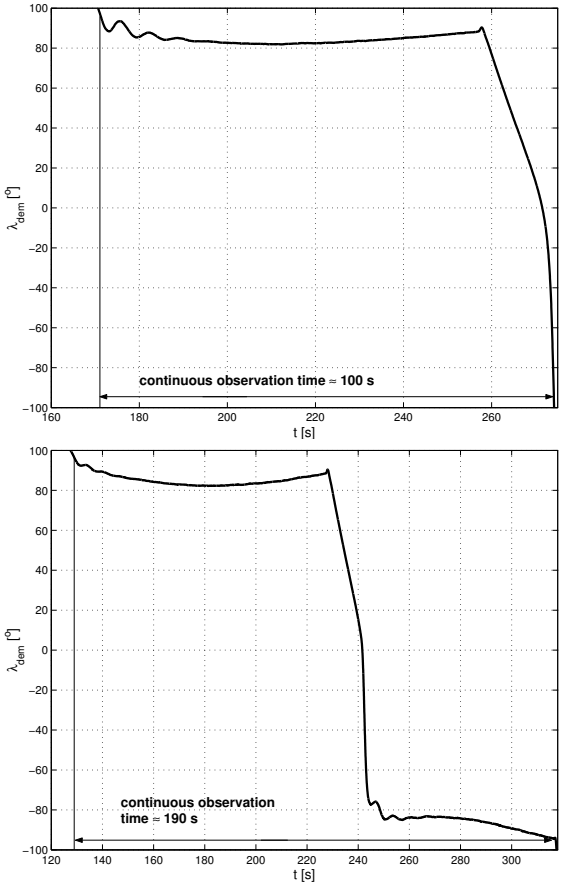

Figure 14 Comparison of Continuous Observation Time of CS1R (top) and CS2R (bottom) Maneuvers

Using a circle-based maneuver and camera limits defined as case 1, this can only be further improved by commanding a smaller radius at each turn until the vehicle's vertical distance from the target is too small to perform the course reversals without leaving the usable segment permanently. The vehicle would then have to return to the first (outermost) radius. This would further increase the continuous observation time, but also the continuous time when the target is not in sight, because the last course reversal back to the first radius would be significantly wider.

Figure 14 shows a direct comparison of the λ time histories of both case-1-maneuvers. With the CS2R maneuver, the continuous observation time is almost doubled compared to the CS1R maneuver. It is therefore the more favorable one.

Case 2: Circle and Ellipse Combination (CEC)

With extended camera motion range ('case 2'), the vehicle does not necessarily have to fly on a circular path at all times in order to obtain target centered images. A modification of the CS1R maneuver can therefore provide continuous observation time with nearly unlimited extent. This modification employs a slower return to the outer radius. For parameterization, an elliptic path is used after the course reversals. These are best done where the distance between the circle and the ellipse is largest, so the size of the usable segment is 180^o.

The parameterization for χ_{dem} is the same as the one for the CS1R maneuver, since the vehicle is supposed to turn towards the target whenever it reaches the boundaries of the usable segment. In this case, the size of the usable segment is set to a fixed value of $\Psi_{US} = \pi$ and $\Psi_{PM} = \Psi_S$. The decision whether the circular or the elliptical path is to be used depends on the following conditions:

1) the difference between the current position and the position of the sun
2) the difference between the current position and the 2π-bound opposite of the position of the sun
3) the current direction of flight (cc or cw)
4) the difference between the middle position of the usable segment and its 2π-bound opposite

The expression for R_{dem} on the elliptical path is obtained by using standard ellipsoid parameters: the size of the semi-major/minor axes (same as R_{out} and R_{in} for CS2R) as well as the angle from the semi-major axis ($\Psi_P - \Psi_S$).

$$R_{dem}(\Psi_P) = \sqrt{\frac{R_{out}^2 R_{in}^2}{R_{out}^2 - \cos^2(\Psi_P - \Psi_S) \cdot \left(R_{out}^2 - R_{in}^2\right)}}$$

The ground track obtained from the simulation is

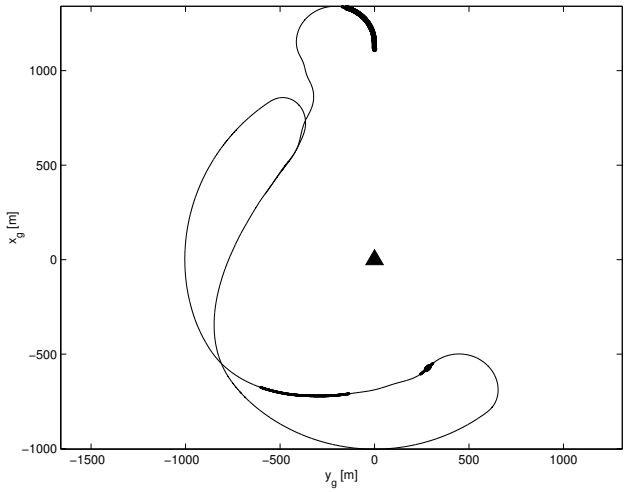

Figure 15 Simulated Ground Track of CEC

shown in figure 15, with highlighting according to the quality of the camera images: centered view of the target (thin line), non-centered view of the target (medium line), target not in sight (thick line), $V_a = 30m/s$, $V_w = 5m/s$, $\Psi_S = 235^o$, $\Psi_w = 90^o$, target at origin. The area of thick highlighting is very small on the actual maneuver pattern, which means that the CEC maneuver provides continuous observation of the target.

Conclusion

It has been shown that Unmanned Air Vehicles equipped with a 2-degree-of-freedom pan-tilt camera can be used for long-term autonomous observation of stationary ground targets. A flight path guidance control has been developed which is mostly independent of a specific model of UAV and

can be applied to any type of flight path as long as the path can be parameterized by a deviation from the desired course and a distance between the vehicle and the desired path. Using differential GPS for the determination of flight path parameters provides accuracy for following linear, circular, and elliptical flight paths. Furthermore, the developed path following guidance law is independent of wind data and not subject to wind estimation errors, which improves accuracy and robustness. The environmental aspects wind and sunlight have an influence on the quality of the images taken by the camera. These influences can set limits to the time span of continuous target observation, especially when the range of camera motion is mechanically limited.

Two different camera limit specifications with realistic applicability have been analyzed for potential problems. Solutions to these problems have been found by applying circle-based flight maneuvers including commanded sideslip for heading adjustment. The different flight maneuvers have been parameterized, simulated, and compared regarding complexity of parameterization, maximum continuous observation time, and distance between target and vehicle. It has been shown that more complex maneuvers provide longer continuous observation time. The best results regarding the observation time have been obtained with wider range of camera motion and the circular-elliptical maneuver, where the continuous observation time is limited by the amount of fuel onboard the vehicle. A minimum of information is required for the parameterization of the maneuver paths and the correct alignment of the camera. This reduces sources of estimation and sensor errors. With autonomous flight path following guidance and camera alignment, the operation of observing a target is significantly simplified.

Acknowledgment

The authors are grateful to Marius Niculescu for providing the Aerosonde dynamic model. The Insitu Group and Hood Technology Corporation supported this work. This work was funded in part by the University of Washington, Royalty Research Fund grant 65–1914.

Nomenclature

Velocities:

V_a	vehicle indicated airspeed
V_c	inertial velocity
V_w	wind speed

Angles:

Ψ	aircraft heading
Ψ_P	'clock angle' (relative bearing from target)
Ψ_w	wind direction
Ψ_S	position of sun relative to target
Ψ_{PM}	middle position of usable circle-segment
Ψ_{US}	size of usable circle-segment
χ	flight path direction, course
Φ	bank angle
Θ	pitch angle
γ	flight path slope
β	sideslip angle
κ	camera tilt angle
λ	camera pan angle
ϵ	geographic longitude
ϕ	geographic latitude

Distance/Position:

x_g	GPS north component
y_g	GPS east component
h	GPS altitude
R	horizontal distance between aircraft and target
Δy	deviation from the desired flight path
R_E	mean radius of the Earth
ΔP	distance between two points with coordinates P[x,y]

Vectors:

$\vec{los}$	line of sight vector
$\vec{cor}$	position of the camera in the body reference frame
$\vec{X}_T$	vector to target location
$\vec{X}_{AC}$	vector to position of the vehicle

Forces:

L	lift
W	weight
Y	side force

Control Derivatives:

$C_{Y\beta}$	derivative of side force with respect to sideslip angle

Aircraft Specific Data:

m	aircraft mass
S	wing surface area

Air Data:

ρ	air density
q_∞	dynamic pressure

Indices:

a	aerodynamic reference frame
b	body reference frame
c	inertial reference frame
g	earth reference frame
w	wind data
T	the target object
AC	the vehicle
cam	camera reference frame
dem	demanded values
com	commanded values

References

[1] P. G. Thomasson, *Guidance of a Roll-Only Camera for Ground Observation in Wind*, from: Journal of Guidance, Control, and Dynamics, Vol. 21, No. 1, January-February 1998, p.39-44

[2] AeroSim Blockset Version 1.0, Unmanned Dynamics LLC, USA, http://www.u-dynamics.com

[3] Aerosonde Ltd, Australia, http://www.aerosonde.com

[4] The Insitu Group, Inc., Bingen, WA, http://www.insitugroup.net/Pages/aerosonde.html

[5] R. Brockhaus, *Flugregelung*, 2nd ed., Springer-Verlag, Berlin Heidelberg, Germany, 2001, p.747

[6] K.Y. Pettersen and E. Lefeber, *Way-point tracking control of ships*, Proc. of the 40th IEEE Conference on Decision and Control, December 2001, pp.940-945,Orlando, FL.

[7] R.Rysdyk, *UAV Path Following for constant line-of-sight*, 2nd AIAA "Unmanned Unlimited" Systems,Technologies, and Operations Aerospace, Land, and Sea Conference, Paper #6626, September, 2003, San-Diego, CA.